ORGANOMETALLICS

Article

pubs.acs.org/Organometallics

Mononuclear (*O,O′* or *N,N′*) and Heterodinuclear (*O,O′* and *N,N′*) Transition-Metal Complexes of *ortho*-Quinoid Bis(pyrazol-1-yl)methane Ligands

Florian Blasberg, Michael Bolte, Hans-Wolfram Lerner, and Matthias Wagner*

Institut für Anorganische und Analytische Chemie, Goethe-Universität Frankfurt, Max-von-Laue-Straße 7, D-60438 Frankfurt (Main), Germany

Supporting Information

ABSTRACT: The *ortho*-hydroquinone-substituted bis(3,5-dimethylpyrazol-1-yl)methane ligand $(HO)_2C_6H_3{-}C(H)(pz^{Me,Me})_2$ (**7**) has been synthesized and fully characterized. Together with its bis(3-*tert*-butylpyrazol-1-yl)methane congener $(HO)_2C_6H_3{-}C(H)(pz^{tBu})_2$ (**6**), **7** was employed in oxidation and complexation studies. **6** has been oxidized with 2,3-dichloro-5,6-dicyano-*para*-benzoquinone to the corresponding *ortho*-benzoquinone form **9** on a preparative scale. Pure samples of **9** are stable for several hours in solution and for approximately one day in the solid state. Attempts at a *N,N′* coordination of $[PdCl_2]$ to **6** led to decomposition of the $-C(H)(pz^{tBu})_2$ moiety, whereas an introduction of $[PdCl_2]$ exclusively at the *N,N′* site was possible in high yield for ligand **7**. A selectively *O,O′*-chelated $[(p\text{-cym})Ru]^{2+}$ complex was accessible for ligand **6**, but not for **7**. In contrast, $[(ppy)_2Ir]^+$ and $[(Cp^*)Ir]^{2+}$ gave *O,O′* complexes with both donors **6** and **7** (Hppy = 2-phenylpyridine; HCp* = pentamethylcyclopentadiene). The heterodinuclear complex $[(Cp^*)Ir(O)_2C_6H_3{-}C(H)(pz^{Me,Me})_2PdCl_2]$ (**16**) was obtained from **14** and $[(MeCN)_2PdCl_2]$.

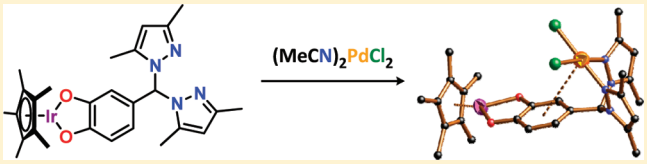

INTRODUCTION

Cooperative catalysis, a phenomenon frequently observed in enzymatic systems,[1−3] has evolved into a guiding principle of catalyst design.[4−6] Two different variants of cooperative substrate activation are commonly observed: (i) cooperation of a transition metal and a redox-active ligand and (ii) cooperation of two or more (different) transition metals.[7]

Case (i) is well represented by the oxidative addition of alkyl halides to a square-planar Co(III) complex with two redox noninnocent amidophenolate ligands, which deliver the electrons for substrate activation. The metal does not change its oxidation state during this process.[8] Case (ii) is illustrated by the asymmetric ring-opening (ARO) of *meso* epoxides with Me_3SiN_3: An ARO catalyst consisting of two covalently tethered chiral [(salen)Cr] complexes is 1−2 orders of magnitude more reactive than the corresponding monomeric complexes.[9]

Our group has a long-standing interest in the properties of complexes showing electronic communication between redox-active ligands and metal ions.[10] Special emphasis has been put on ferrocene- or quinone-containing oligotopic poly(pyrazol-1-yl)borate[11,12] and bis(pyrazol-1-yl)methane ligands[13−17] (note: in this paper, the general term "quinone" or "quinoid" will be used whenever the oxidation state of any derivative of *ortho*-hydroquinone/*ortho*-benzoquinone does not need to be specified). Using the *para*-naphthoquinone-substituted bis(pyrazol-1-yl)methane Pd(II) complex **1** (Scheme 1), we were able to prove the formation of a *para*-naphthosemiquinonate anion (**3**), following selective Pd(II) → Pd(0) reduction (**1** → **2**).[15] Thus, electron transfer from Pd(0) to a *para*-benzoquinone moiety is obviously possible through space, without direct coordination of the metal atom to the organic redox-active fragment.

Considering that electron transfer can proceed in both directions, from the metal to the ligand and vice versa, we recently set out to develop synthetic routes to (hetero)-dimetallic complexes featuring redox-active quinoid bis(pyrazol-1-yl)methane linkers for potential applications in combined redox-/transition metal-mediated catalysis (cf. **4**−**7**; Scheme 1). To this end, the *para*-quinone redox reservoirs were replaced by *ortho*-quinones. The latter provide a chelating coordination site of their own, which (i) greatly differs from the bis(pyrazol-1-yl)methane donor set (i.e., *O,O′* vs *N,N′*), (ii) improves metal ↔ ligand electron transfer due to direct conjugation, and (iii) decouples electron from proton transfer in the *O,O′* complexes.

The purpose of this paper is to report on selected mononuclear and heterodinuclear transition-metal complexes of *ortho*-quinoid bis(pyrazol-1-yl)methane ligands with substituents of varying steric demand about the *N,N′* coordination site. The ligand design was guided by the observation that an increasing bulk of the pyrazolyl substituents leads to improved solubility and to kinetic stabilization of both the *N,N′*-complexed metal ion and the *ortho*-benzoquinone state of the ligand. As a drawback, it renders the bis(pyrazol-1-yl)methane moieties more prone to Lewis acid-induced degradation so that the steric requirements of the ligand have to be properly

Received: January 31, 2012
Published: March 20, 2012

   dx.doi.org/10.1021/om3000746 | *Organometallics* 2012, 31, 3213−3221

Scheme 1. *para*-Naphthoquinone Bis(pyrazol-1-yl)methane Complex 1, Its Selective Pd(II) → Pd(0) Reduction with NEt_3, and the Spectroscopically Observed *para*-Naphthosemiquinonate Pd(I) Complex 3, as Well as the *ortho*-Quinoid Bis(pyrazol-1-yl)methane Ligands 4–7

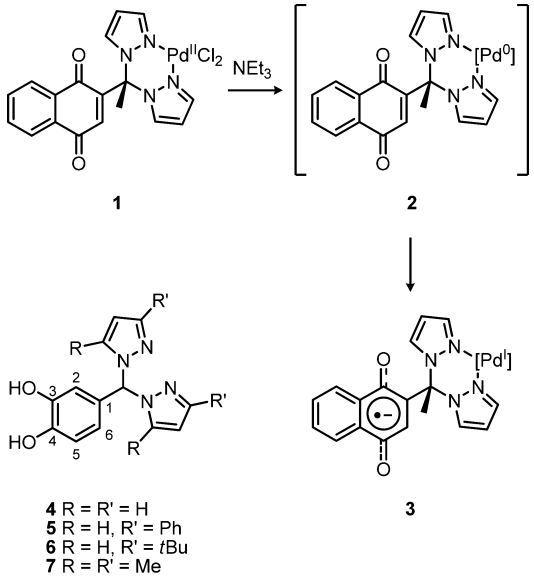

balanced. The coordination behavior was first studied with a special emphasis on the selective introduction of *one* given metal complex fragment at *either* the *O,O′ or* the *N,N′* coordination site. In the second step, we used the knowledge gained by these experiments for the targeted preparation of a hetero*dinuclear* species.

RESULTS AND DISCUSSION

Synthesis, Characterization, and Chemical Oxidation of Substituted *ortho*-Quinoid Bis(pyrazol-1-yl)methane Ligands. Compound **7** was synthesized starting from 3,4-dihydroxybenzaldehyde and $(pz^{Me,Me})_2SO$ in a similar way to the *ortho*-quinoid bis(pyrazol-1-yl)methane ligands **4**, **5**, and **6**[17] (Scheme 1; $pz^{Me,Me}$ = 3,5-dimethylpyrazol-1-yl). The ^1H and ^{13}C NMR spectra (d_6-DMSO) of **7** show no peculiarities compared to the related species **4**–**6** and therefore do not merit further discussion.

To further corroborate the proposed ligand structure, crystals of **7**, grown from a saturated $MeCN/C_6H_6$ solution, were investigated by X-ray diffraction (Figure 1, Table 1). Key metrical parameters, namely, C–O single bonds (av 1.369(2) Å; cf. *ortho*-hydroquinone: av 1.371 Å[18] vs *ortho*-benzoquinone: 1.220 Å[19]) and a small spread of C–C bond lengths (1.380(3)–1.402(3) Å) indicate the presence of an *ortho*-hydroquinone moiety. Thus, as already evidenced by the NMR spectroscopic results, no air oxidation had taken place.

Since the redox properties of the ligands are particularly relevant in the context of this paper, we next studied the electrochemical behavior of ligand **6**, which possesses the highest solubility of the four derivatives in all common organic solvents.

In cyclic voltammetric experiments (DMF, 0.1 M $[Bu_4N][PF_6]$), **6** is irreversibly oxidized at a peak potential of 0.63 V (vs FcH/FcH^+, scan rate = 200 mV s^{-1}; cf. the Supporting Information (SI) for a plot of the cyclic voltammogram). When, after oxidation, the sweep is continued into the cathodic regime, an irreversible reduction wave appears at a peak potential of −0.54 V.

The parent *ortho*-benzoquinone readily decomposes under ambient conditions.[19,20] It therefore had to be clarified by chemical oxidation and analysis of the product(s) whether the irreversibility of the redox transitions of **6** is simply due to loss of O*H* protons or whether a more severe structural reorganization takes place.

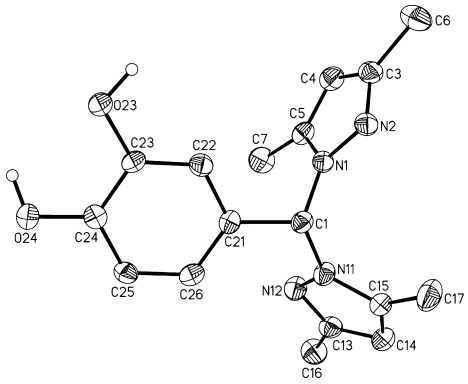

Figure 1. Molecular structure of ligand **7** (50% displacement ellipsoids; H atoms, except for OH groups, omitted for clarity). Selected bond lengths [Å], bond angles [deg], torsion angles [deg], and dihedral angles [deg]: C1–N1 1.466(3), C1–N11 1.453(2), C1–C21 1.527(2), C23–O23 1.372(2), C24–O24 1.365(2); N1–C1–N11 112.2(2), N1–C1–C21 111.4(2), N11–C1–C21 114.7(2); C21–C1–N1–N2 116.5(2), C21–C1–N11–N12 47.2(2); HQ//pz(N1) 78.4, HQ//pz(N11) 53.2, pz(N1)//pz(N11) 69.4.

Table 1. Selected Crystallographic Data and Structure Refinement Details for 7 and 10

	7	10
formula	$C_{17}H_{20}N_4O_2$	$C_{17}H_{20}Cl_2N_4O_2Pd{\cdot}EtOH$
fw	312.37	535.74
color, shape	colorless parallelogram	yellow-brown plate
temp (K)	173(2)	173(2)
radiation	Mo Kα, 0.71073 Å	Mo Kα, 0.71073 Å
cryst syst	monoclinic	monoclinic
space group	$P2/n$	$P2_1$
a (Å)	9.8973(9)	9.1607(4)
b (Å)	7.4957(4)	14.1667(8)
c (Å)	21.100(2)	9.6108(4)
α (deg)	90.00	90.00
β (deg)	93.407(7)	114.902(3)
γ (deg)	90.00	90.00
V (Å^3)	1562.6(2)	1131.30(9)
Z	4	2
$D_{calcd.}$ (g cm^{-3})	1.328	1.573
$F(000)$	664	544
μ (mm^{-1})	0.090	1.083
cryst size (mm)	0.25 × 0.18 × 0.17	0.50 × 0.35 × 0.12
no of rflns coll	11 340	15 962
no of indep rflns (R_{int})	2914 (0.0925)	4518 (0.0598)
data/restr/params	2914/0/221	4518/1/269
GOOF on F^2	0.904	1.022
R_1, wR_2 ($I > 2\sigma(I)$)	0.0449, 0.0930	0.0330, 0.0843
R_1, wR_2 (all data)	0.0787, 0.1026	0.0332, 0.0845
largest diff peak and hole (e Å^{-3})	0.190, −0.232	0.686, −0.920

dx.doi.org/10.1021/om3000746 | *Organometallics* 2012, 31, 3213–3221

Under the reaction conditions typically applied for oxidizing hydroquinones (i.e., $[Ce(NH_4)_2(NO_3)_6]$ = CAN; MeCN/H_2O), only product mixtures were obtained; the same was true for other strong oxidants such as Pb(IV) and Ag(I). However, after **6** was treated with CAN in the presence of excess 4-*tert*-butylpyridine, the pyridinium salt **8** could be isolated in single-crystalline form (Scheme 2; cf. the SI for more information

Scheme 2. Oxidation of 6 to 9 and Trapping of 9[a]

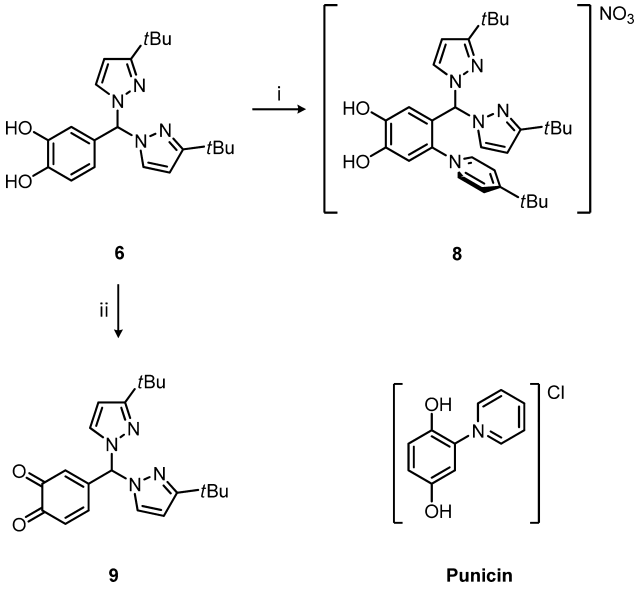

[a]Conditions: (i) 3 equiv of CAN, 5 equiv of 4-*t*Bu-pyridine, MeCN/H_2O 2:1, rt, 75 min; (ii) 1 equiv of DDQ, C_6H_6, rt, 2 min. CAN = $[Ce(NH_4)_2(NO_3)_6]$, DDQ = 2,3-dichloro-5,6-dicyano-*para*-benzoquinone.

including an X-ray crystal structure determination). This trapping experiment, which was inspired by the synthesis of the alkaloid punicin (Scheme 2) from *para*-benzoquinone and pyridine,[21−23] indirectly proves the intermediate formation of the *ortho*-benzoquinone **9** and shows that it is sufficiently stable to be used for further derivatization.

Finally, we found that DDQ (2,3-dichloro-5,6-dicyano-*para*-benzoquinone) cleanly and quantitatively oxidizes **6** to **9**. The key to success was the application of C_6H_6 as the solvent, which allowed for facile separation of the insoluble reduced side product $DDQH_2$. Following this protocol, **9** can be prepared in high purity and either used immediately as C_6H_6 solution or isolated as a finely divided powder after freeze-drying.[24]

The NMR spectroscopic characteristics of **9** are in accord with a bis(3-*tert*-butylpyrazol-1-yl)methane-substituted *ortho*-benzoquinone. Especially the ^{13}C NMR shift values of the carbonyl groups (178.8, 179.2 ppm; C_6D_6) serve as clear indicators of a successful oxidation (cf. **6**: HQ-C3,4 = 145.7, 146.1 ppm; C_6D_6; cf. SI). In the solid state, **9** decomposes within one day, even under an argon atmosphere; in C_6H_6 solution the decomposition is complete after a few hours (NMR spectroscopic control).

Selective Introduction of Transition Metals at Either Coordination Site of *ortho*-Quinoid Bis(pyrazol-1-yl)-methane Ligands 6 and 7. Exploratory screening experiments with the ligands **4**−**7** and various soluble $Pd(II)Cl_2$ sources revealed that **7** provides far better solubility than **4** and does not show the problems of bis(pyrazol-1-yl)methane decomposition[17] that we had been encountering with **5** and **6**. For this reason, ligand **7** was employed in most of the complexation experiments throughout this study.

Selective *N,N′* coordination of a $[PdCl_2]$ moiety was achieved in high yield under base-free conditions using **7** and $[(MeCN)_2PdCl_2]$ (cf. **10**; Scheme 3). The ^1H NMR

Scheme 3. Preparation of Palladium Complex 10[a]

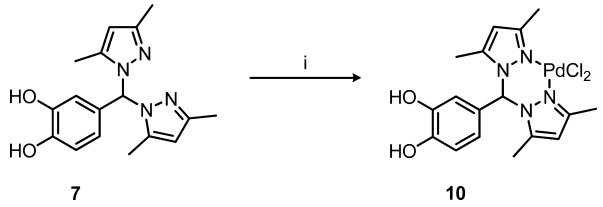

[a]Conditions: (i) 1 equiv of $[(MeCN)_2PdCl_2]$, MeCN, rt, 2.5 h.

spectroscopic properties (d_3-MeCN) of **10** are unexceptional, the only remarkable feature being the presence of two OH resonances at 6.86 and 7.15 ppm, consistent with the proposed *N,N′* binding mode. The X-ray crystal structure determination of **10** (Figure 2, Table 1) reveals a *cis*-N_2PdCl_2 fragment with a

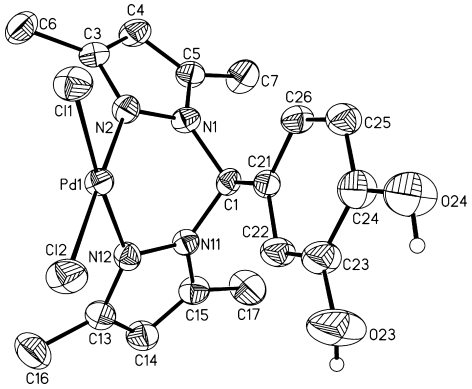

Figure 2. Molecular structure of palladium complex **10** (50% displacement ellipsoids; H atoms, except for OH groups, omitted for clarity). Selected bond lengths [Å], bond angles [deg], torsion angles [deg], and dihedral angles [deg]: Pd1−Cl1 2.291(1), Pd1−Cl2 2.290(1), Pd1−N2 2.013(2), Pd1−N12 2.047(3), Pd1···COG(HQ) 3.76, C1−N1 1.464(4), C1−N11 1.449(4), C1−C21 1.529(4), C23−O23 1.360(5), C24−O24 1.371(4); Cl1−Pd1−Cl2 90.2(1), Cl1−Pd1−N2 90.6(2), Cl2−Pd1−N12 92.8(1), N2−Pd1−N12 86.3(2), N1−C1−N11 109.0(2), N1−C1−C21 112.4(2), N11−C1−C21 111.5(2); Cl1−Pd1−N2−N1 131.5(2), Cl2−Pd1−N12−N11 −136.7(2), C21−C1−N1−N2 −66.1(4), C21−C1−N11−N12 64.0(3); HQ//pz(N1) 87.9, HQ//pz(N11) 75.9, pz(N1)//pz(N11) 65.5. COG = ring centroid.

square-planar configuration. The Pd(II) ion is located in close proximity to the hydroquinone π face (Pd1···COG(HQ) = 3.76 Å; COG = ring centroid). The Pd−Cl (av 2.291(1) Å) and Pd−N (av 2.030(3) Å) bond lengths compare well with other published $[(R)(H)C(pz^{Me,Me})PdCl_2]$ complexes.[25]

Having established selective *N,N′* complexation, we next turned our attention to the *O,O′* coordination site. Ruthenium and iridium are both catalytically active metals,[26] of which *ortho*-quinone complexes are known[27] and which were therefore chosen for further investigations. Since metal binding at the *O,O′* position requires a base to capture the OH protons, several Brønsted bases were screened with the focus on easily

dx.doi.org/10.1021/om3000746 | *Organometallics* 2012, 31, 3213−3221

separable conjugated acids. The presence of thallium cations in combination with metal chloride precursors proved beneficial for M−O bond formation, because TlCl precipitation provides a strong thermodynamic driving force. Thus, basic thallium species appeared to be the reagents of choice. In order to circumvent the highly toxic, volatile TlOEt, the crystalline base TlO*t*Bu[28] was used instead.

As a versatile precursor of ruthenium complex fragments, $[(p\text{-cym})RuCl_2]_2$ (*p*-cym = *para*-cymene = 1-isopropyl-4-methylbenzene) was selected for complexation with **7**. The purple solid isolated from the reaction mixture gave only broad resonances in the NMR spectra (d_8-THF), which therefore did not provide sufficient information for a definite assignment of the product as [(*p*-cym)Ru(**7**)]. Numerous crystallization attempts also remained unsuccessful. Two different explanations for the special NMR features observed can be envisioned. One would be the formation of paramagnetic compounds. If this was the case, the amount of these impurities would have to be small, because the broad resonances appear in the same shift regions as the signals of the $[(p\text{-cym})Ru]^{2+}$ complex **11** discussed below. Alternatively, the $[(p\text{-cym})Ru]^{2+}$ fragment in hypothetical [(*p*-cym)Ru(**7**)] might undergo a dynamic association−dissociation equilibrium, possibly even with scrambling between the *O*,*O*′ and *N*,*N*′ coordination sites.

As a test for this assumption, we repeated the experiment with the sterically more congested *t*Bu ligand **6**, which should favor *O*,*O*′ over *N*,*N*′ binding (Scheme 4). Now, the reaction

Scheme 4. Synthesis of Ruthenium and Iridium Complexes 11−15[a]

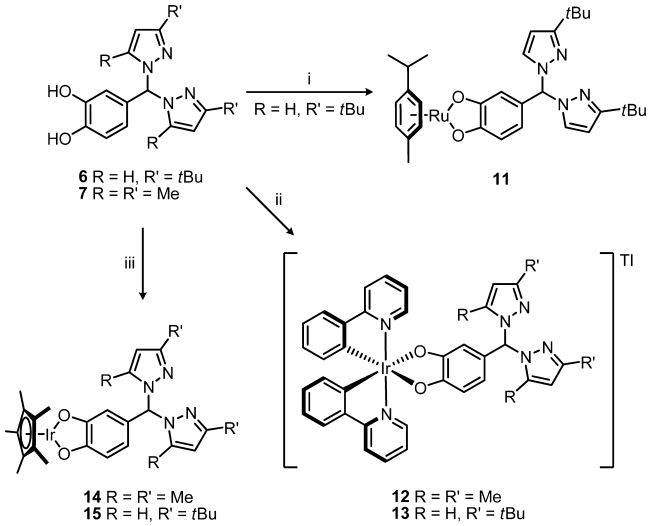

[a]Conditions: (i) 2 equiv of TlO*t*Bu, 0.5 equiv of $[(p\text{-cym})RuCl_2]_2$, THF, rt, 12 h; (ii) 2 equiv of TlO*t*Bu, 0.5 equiv of $[(ppy)_2IrCl]_2$, THF, rt, 12 h; (iii) 2 equiv of TlO*t*Bu, 0.5 equiv of $[(Cp^*)IrCl_2]_2$, THF, rt, 12 h. *p*-cym = 1-isopropyl-4-methylbenzene, Hppy = 2-phenylpyridine, HCp* = pentamethylcyclopentadiene.

proceeded smoothly to provide analytically pure **11** in essentially quantitative yield. The ^{1}H NMR spectrum (d_8-THF) of **11** is characterized by the absence of OH resonances and the presence of signals assignable to $[(p\text{-cym})Ru]^{2+}$ as well as deprotonated **6** in a 1:1 ratio. In the ^{13}C NMR spectrum (d_8-THF) we find, compared to free **6**, a notable 20 ppm downfield shift of the oxygen-carrying carbon atoms HQ-C3,4 (164.3, 165.0 ppm; cf. the SI for the result of an X-ray crystal structure determination of **11**).

Even though the successful synthesis of **11** can be regarded as an important proof of concept, the compound itself is only of limited practical use in the present context, because we have previously shown that ligand **6** decomposes upon treatment with, for example, $[(MeCN)_2PdCl_2]$.[17] We therefore looked for alternative complex fragments allowing for exclusive *O*,*O*′ coordination, not only in the case of the sterically congested ligand **6** but also in the case of **7**. For our purposes, $[(ppy)_2IrCl]_2$ (Hppy = 2-phenylpyridine) appeared to be a convenient starting material, easily prepared in gram quantities.[29] The reactions of **7** and **6** first with TlO*t*Bu and then with $[(ppy)_2IrCl]_2$ yield, after workup, the desired *ortho*-hydroquinonate iridium(III) complexes **12** and **13** (Scheme 4) in excellent yields as their thallium salts. The octahedral iridium complexes are chiral and have a fixed configuration (*cis*-*C*,*C*).[30] Thus, two isomers form after addition to the nonsymmetric ligands **7** and **6**, as is evident from the fact that two signal sets of equal intensity are visible both in the ^{1}H and in the ^{13}C NMR spectra of analytically pure samples. The NMR spectra are further characterized by broad line widths and unusually highfield-shifted *ortho*-hydroquinonate proton resonances. We tentatively attribute these features to the presence of dynamic Tl(I)-bridged aggregates (cf. the solid-state structure of $(\mathbf{12})_2$ below).

Compound **12** crystallizes from an EtCN solution in the form of doubly Tl(I)-bridged dimers $(\mathbf{12})_2$ (Figure 3; Table 2). As planned, octahedrally coordinated $[(ppy)_2Ir]^+$ ions reside exclusively at *O*,*O*′ sites (av Ir−O = 2.145(8) Å; cf. 2.113(3) Å for a $[(Cp^*)Ir(III)]^{2+}$ biphenolate complex[31]). Tl1 is

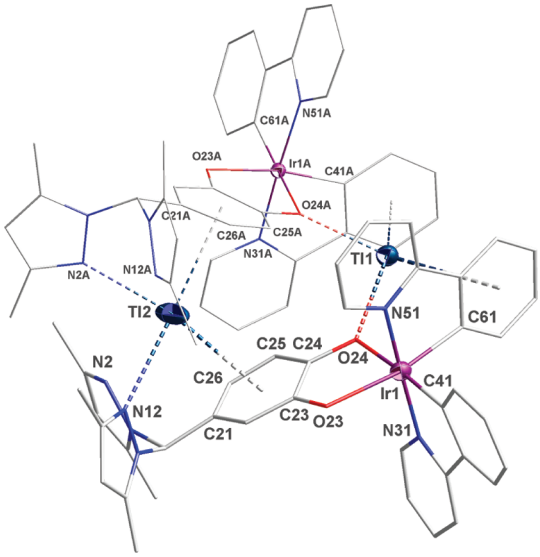

Figure 3. POV-ray representation of the dimer $(\mathbf{12})_2$ in the solid state (H atoms omitted for clarity). Selected bond lengths [Å] and bond angles [deg] are given for both monomers of $(\mathbf{12})_2$: Ir1−O23 2.143(8), Ir1−O24 2.143(8), Ir1−N31 2.034(11), Ir1−N51 2.015(11), Ir1−C41 1.976(13), Ir1−C61 2.009(13), Ir1A−O23A 2.136(8), Ir1A−O24A 2.157(8), Ir1A−N31A 2.050(11), Ir1A−N51A 2.047(11), Ir1A−C41A 2.000(12), Ir1A−C61A 2.019(12), Tl1−O24 2.505(8), Tl1−O24A 2.488(8), Tl1···COG(C61) 3.471, Tl1···COG(C41A) 3.478, Tl2−N12 2.837(12), Tl2−N2A 2.823(10), Tl2···COG(C21) 3.171, Tl2···COG(C21A) 3.012; O23−Ir1−O24 79.5(3), O23A−Ir1A−O24A 79.0(3). COG = ring centroid.

dx.doi.org/10.1021/om3000746 | *Organometallics* 2012, 31, 3213−3221

Table 2. Selected Crystallographic Data and Structure Refinement Details for $(12)_2$, 14, and 16

	$(12)_2$	14	16
formula	$C_{78}H_{68}Ir_2N_{12}O_4Tl_2 \cdot 3EtCN$	$C_{27}H_{33}IrN_4O_2 \cdot 3THF$	$C_{27}H_{33}Cl_2IrN_4O_2Pd \cdot THF \cdot 0.5H_2O$
fw	2195.82	854.09	896.19
color, shape	red plate	red plate	red block
temp (K)	173(2)	173(2)	173(2)
radiation	Mo Kα, 0.71073 Å	Mo Kα, 0.71073 Å	Mo Kα, 0.71073 Å
cryst syst	triclinic	triclinic	monoclinic
space group	$P\bar{1}$	$P\bar{1}$	$C2/c$
a (Å)	14.2553(6)	8.7625(6)	21.5132(8)
b (Å)	17.3216(7)	12.9304(10)	14.3154(3)
c (Å)	17.9782(8)	17.2848(13)	22.5580(8)
α (deg)	101.431(4)	90.590(6)	90.00
β (deg)	102.004(3)	101.634(6)	102.434(3)
γ (deg)	91.638(3)	95.570(6)	90.00
V (Å^3)	4244.8(3)	1908.2(2)	6784.2(4)
Z	2	2	8
$D_{calcd.}$ (g cm^{-3})	1.718	1.486	1.755
$F(000)$	2116	872	3528
μ (mm^{-1})	6.967	3.545	4.645
cryst size (mm)	0.17 × 0.05 × 0.04	0.27 × 0.18 × 0.08	0.35 × 0.20 × 0.15
no of rflns coll	52 244	23 748	32 784
no of indep rflns (R_{int})	15871 (0.1132)	6735 (0.1098)	6348 (0.0661)
data/restr/params	15871/66/986	6735/15/451	6348/1/407
GOOF on F^2	0.754	0.926	1.024
R_1, wR_2 ($I > 2\sigma(I)$)	0.0531, 0.1156	0.0527, 0.1116	0.0344, 0.0722
R_1, wR_2 (all data)	0.0976, 0.1255	0.0760, 0.1179	0.0452, 0.0753
largest diff peak and hole (e Å^{-3})	2.405, −3.277	2.270, −2.487	0.610, −1.498

surrounded in a distorted tetrahedral fashion by two oxygen atoms of two different *ortho*-hydroquinonate moieties (i.e., O24, O24A) and by the centroids of the C_6H_4 rings containing C61 and C41A. The average Tl1−O distance of 2.496(8) Å is comparable to those of other mixed thallium/metal μ-alkoxides;[32] in contrast, the average Tl1···COG distance of 3.475 Å is longer than the average Tl···COG contact found in $[Tl(toluene)_2]^+$ (3.04 Å).[33] Tl2 establishes the four closest contacts to two nitrogen atoms of two different bis(pyrazol-1-yl)methane ligands (i.e., N12, N2A) and to the centroids of both *ortho*-hydroquinonate rings. In this case, the ligand environment comes close to a square-planar arrangement. The Tl2−N bonds (av value: 2.830(12) Å) are somewhat longer than in a related scorpionate ligand containing a Tl···Ph (2.959 Å) and a Tl−N(pz) contact (2.579(5) Å).[34]

The $[(ppy)_2Ir]^+$ fragment is compatible with ligand **7** (rather than with only **6**, as was $[(p\text{-cym})Ru]^{2+}$), and, consequently, further coordination of $[PdCl_2]$ at the *N*,*N*′ site of the resulting compound **12** should be achievable. Unfortunately, the use of $[(ppy)_2Ir]^+$ brings about the new disadvantage of isomer formation, which arises from its chirality and complicates its NMR spectra but does not rule out its potential use as, for example, a light-harvesting group. At the present stage, however, we found it more important to be able to readily characterize new compounds by NMR spectroscopy rather than to establish certain functionalities and therefore turned our attention to $[(Cp^*)Ir]^{2+}$ (HCp* = pentamethylcyclopentadiene). The 16 VE iridium complexes **14**/**15** (Scheme 4) were readily accessible from $[(Cp^*)IrCl_2]_2$ and **7**/**6** in the presence of 2 equiv of Tl*O*t*Bu*.

The aimed-for *O*,*O*′ coordination mode is once again evident from missing OH resonances in the ^{1}H NMR spectra (d_8-THF) of **14** and **15**. Since all signals are narrow and well resolved, coordination site scrambling of the metal ion, as had likely taken place in $[(p\text{-cym})Ru(7)]$, appears not to be an issue here. Downfield-shifted signals of the HQ carbon atoms C3 and C4 (165.0, 165.2 ppm for **14**; 165.0, 165.6 ppm for **15**) are present in the ^{13}C NMR spectra following Ir(III) coordination.

Complex **14**, which crystallizes from THF together with three equivalents of THF, was structurally characterized by X-ray crystallography (Figure 4, Table 2; cf. the SI for the result of an X-ray crystal structure determination of **15**). The Ir(III) center is chelated by the two oxygen atoms of the *ortho*-hydroquinonate moiety and adopts a two-legged piano stool configuration; no close contacts of cocrystallized THF

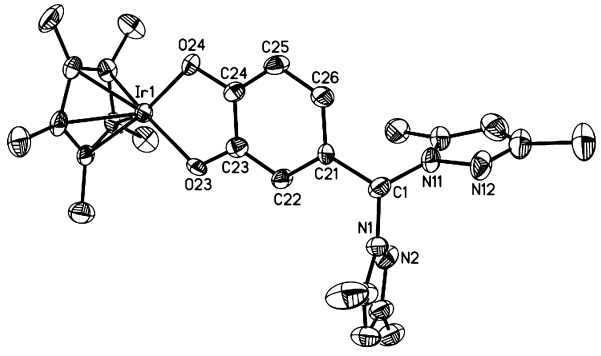

Figure 4. Molecular structure of the iridium complex **14** (50% displacement ellipsoids; H atoms omitted for clarity). Selected bond lengths [Å], bond angle [deg], and dihedral angles [deg] for **14**: Ir1−O23 1.979(6), Ir1−O24 1.991(6), Ir1···COG(Cp*) 1.78, C23−O23 1.361(10), C24−O24 1.358(9); O23−Ir1−O24 81.3(2); HQ//pz(N1) 80.2, HQ//pz(N11) 79.3, pz(N1)//pz(N11) 78.8. COG = ring centroid.

dx.doi.org/10.1021/om3000746 | *Organometallics* 2012, 31, 3213−3221

molecules are found in the solid state. The average Ir−O bond length amounts to 1.985(6) Å; the distance between the iridium ion and the centroid of the Cp* ligand is 1.78 Å (cf. 1.75 Å for a $[(Cp^*)Ir(III)]^{2+}$ biphenolate complex[31]). Apart from slightly contracted C−O bonds, the *O,O′/N,N′* ligand framework of **14** shows only minor deviations in bond lengths and bond angles compared to the free ligand **7** (Figure 1).

Complex **14** was also investigated by cyclic voltammetry (DMF, 0.1 M $[Bu_4N][PF_6]$). A reduction wave appears at $E_{1/2}$ = −2.10 V, which reveals features of electrochemical reversibility; that is, the peak-to-peak separation (ΔE = 78 mV) does not deviate from the value found for the internal ferrocene standard (ΔE(FcH) = 78 mV), and the current ratio i_{pc}/i_{pa} is close to 1, at least at high scan rates (cf. the SI for a plot of the cyclic voltammogram). A comparable reduction event at a potential value of $E_{1/2}$ = −2.11 V (vs FcH/FcH^+) has been reported for the iridium dithiolene complex $[(Cp^*)Ir(S_2C_2(COOMe)_2)]$.[35] For **14**, a second reversible electron transition takes place at $E_{1/2}$ = −0.18 V (ΔE = 97 mV), which we tentatively assign to the *ortho*-hydroquinonate → *ortho*-semiquinonate oxidation.

Preparation of a Heterodimetallic Complex. After the selective synthesis of either *N,N′*- or *O,O′*-coordinated mononuclear complexes (i.e., **10** and **14**, respectively), the targeted preparation of a heterodinuclear species combining both structural motifs was attempted next.

Starting from palladium complex **10**, it was not possible to coordinate $[(Cp^*)Ir]^{2+}$ to the *ortho*-hydroquinonate donor, because unwanted side reactions prevailed (Scheme 5).[36] The alternative approach, i.e., reaction of $[(MeCN)_2PdCl_2]$ with the $[(Cp^*)Ir]^{2+}$ complex **14** (MeCN, 150 °C; sealed tube), led to full consumption of the starting materials within minutes under formation of the Pd(II)/Ir(III) complex **16** in ca. 90% purity (NMR spectroscopic control; Scheme 5). Crystallization from THF afforded analytically pure **16** in good yield.

Scheme 5. Synthesis of the Pd(II)/Ir(III) Complex 16[a]

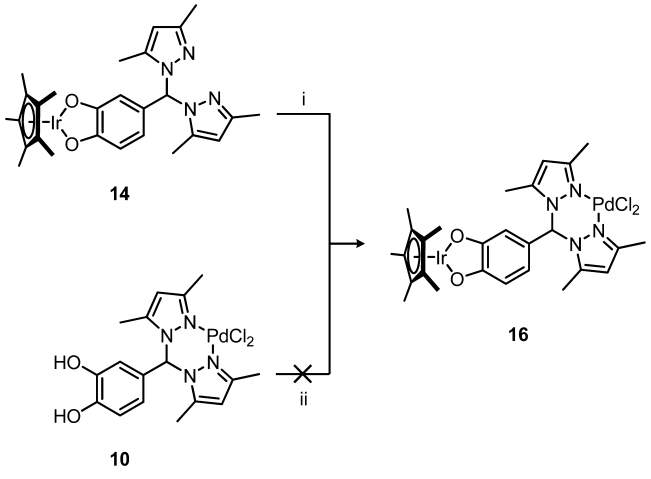

[a]Conditions: (i) 1 equiv of $[(MeCN)_2PdCl_2]$, d_3-MeCN, 150 °C, 2 min; (ii) 2 equiv of LiO*t*Bu, 0.5 equiv of $[(Cp^*)IrCl_2]_2$, THF, rt, 12 h.

The ^1H and ^{13}C NMR spectroscopic data of **16** gave no indication of coordination site scrambling. All key changes in the NMR spectroscopic parameters that are observed upon going from the free ligand **7** to the Pd(II) complex **10** or the Ir(III) complex **14** are well reproduced in the NMR spectra of the Pd(II)/Ir(III) complex **16**.

In order to gain conclusive evidence for the proposed *N,N′*-Pd/*O,O′*-Ir coordination mode, the molecular structure of **16** was determined by X-ray diffraction on a single crystal grown from a THF solution (Figure 5, Table 2). The Pd−N (av 2.042(4) Å) and Pd−Cl bond lengths (av 2.285(1) Å) are similar to those in **10**, and the same holds true for the Ir−O bonds (av 1.995(4) Å) when compared to **14**. As was the case for **10**, the bis(pyrazol-1-yl)methane donor brings the Pd(II) ion in proximity to the π face of the *ortho*-hydroquinonate moiety.

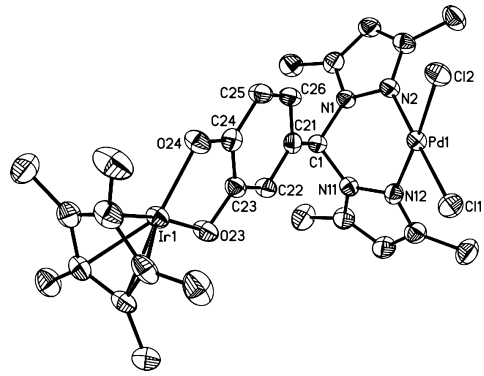

Figure 5. Molecular structure of the palladium/iridium complex **16** (50% displacement ellipsoids; H atoms omitted for clarity). Selected bond lengths [Å], bond angles [deg], and dihedral angles [deg]: Ir1−O23 1.993(4), Ir1−O24 1.997(3), Ir1···COG(Cp*) 1.76, Pd1−Cl1 2.287(1), Pd1−Cl2 2.283(1), Pd1−N2 2.053(4), Pd1−N12 2.030(4), Pd1···COG(HQ) 3.95; O23−Ir1−O24 80.9(1), Cl1−Pd1−Cl2 89.53(5), Cl1−Pd1−N12 91.9(1), Cl2−Pd1−N2 91.9(1), N2−Pd1−N12 86.8(2); HQ//pz(N1) 78.3, HQ//pz(N11) 84.1, pz(N1)//pz(N11) 61.8. COG = ring centroid.

The cyclic voltammogram of **16** (DMF, 0.1 M $[Bu_4N][PF_6]$) shows essentially the same two redox events as the mononuclear Ir(III) complex **14**. In addition, a very broad irreversible feature with an onset at E = −1.30 V appears, which is likely due to Pd(II) reduction (vs FcH/FcH^+; cf. the SI for a plot of the cyclic voltammogram).

CONCLUSION

The *ortho*-hydroquinone-substituted bis(3,5-dimethylpyrazol-1-yl)methane $(HO)_2C_6H_3-C(H)(pz^{Me,Me})_2$ (**7**) provides a versatile ligand platform for the synthesis of *O,O′*- or *N,N′*-coordinated mononuclear complexes as well as *O,O′/N,N′*-bonded heterodinuclear aggregates. A $[PdCl_2]$ fragment attached to the *N,N′* site of **7** resides directly above the *ortho*-hydroquinone π face (at least in the solid state) and is therefore able to electronically interact with the redox-active linker through space. In contrast, $[(p\text{-cym})Ru]^{2+}$, $[(ppy)_2Ir]^+$, and $[(Cp^*)Ir]^{2+}$ complexes chelated by the *O,O′* site are capable of metal ↔ ligand d(π)−p(π) interaction. The redox properties of the new ligand class were studied using the *tert*-butyl derivative $(HO)_2C_6H_3-C(H)(pz^{tBu})_2$ (**6**), because it possesses a higher solubility and kinetic stability of its *ortho*-benzoquinone form than **7**. The free ligand **6** undergoes an irreversible two-electron oxidation at a peak potential of 0.63 V (vs FcH/FcH^+). Since it was possible to synthesize the *ortho*-benzoquinone form **9** of **6** by chemical oxidation on a preparative scale, we conclude that the irreversibility of the oxidation event under the conditions of cyclic voltammetry is solely due to the loss of OH protons. After *O,O′* coordination

dx.doi.org/10.1021/om3000746 | *Organometallics* 2012, 31, 3213−3221

of $[(Cp^*)Ir]^{2+}$, an oxidation event can be observed already at a potential value of $E_{1/2} = -0.18$ V. In this case, electron transfer is no longer coupled to proton transfer and the electron transition becomes reversible. The heterodinuclear complex $[(Cp^*)Ir(O)_2C_6H_3-C(H)(pz^{Me,Me})_2PdCl_2]$ (**16**) meets important structural requirements not only for ligand ↔ metal but also for metal ↔ metal electron transfer: (i) the close proximity of one metal (Pd) to the *ortho*-hydroquinone π face and (ii) the direct conjugation of the other metal (Ir) with the *ortho*-hydroquinone via the oxygen donors.

In the future, we will employ the *O,O′*-bonded metal center as a handle to fine-tune the redox behavior of the ligand and thereby to influence the (catalytic) activity of the metal center residing at the *N,N′* site. In this context, special emphasis will be put on $[(ppy)_2Ir]^+$ and related species, which can act as light-harvesting antennas.

EXPERIMENTAL PART

General Considerations. If not explicitly mentioned otherwise, all reactions and manipulations of air-sensitive compounds were carried out under dry, oxygen-free nitrogen by using standard Schlenk ware or in an argon-filled glovebox. THF, d_8-THF, C_6H_6, C_6D_6, and pentane were freshly distilled under argon from Na/benzophenone. DMF, MeCN, d_3-MeCN, and EtCN were dried over molecular sieves (4 Å) for at least two days, distilled, degassed by three freeze−pump−thaw cycles, and stored in Young's valve ampules. NaH was used as a 60% per weight suspension in mineral oil (commercially available); however, throughout the Experimental Part, all weighed-out quantities refer to neat NaH. **6**,[17] TlO*t*Bu,[28] and $[(ppy)_2IrCl]_2$[29] were prepared according to literature procedures.

1D and 2D NMR spectra were recorded on Bruker AM-250, Bruker Avance-300, and Bruker Avance-400 spectrometers. Chemical shifts are given in ppm and are referenced to residual solvent signals ($^1H/^{13}C\{^1H\}$: C_6D_6: 7.16/128.06; d_8-THF: 1.72, 3.58/25.31, 67.21; d_6-DMSO: 2.50/39.52; d_3-MeCN: 1.94/1.32, 118.26). Abbreviations: s = singlet; d = doublet; dd = doublet of doublets; ddd = doublet of doublets of doublets; m = multiplet; sept = septet; bs = broad singlet; n.r. = multiplet not fully resolved; n.o. = signal expected in the NMR spectrum, but not observed; pz = (substituted) pyrazol-1-yl; HQ = *ortho*-hydroquinone core; BQ = *ortho*-benzoquinone core.

Elemental analyses were performed by the Microanalytical Laboratory of the University of Frankfurt or the Mikroanalytisches Labor Pascher, Remagen, Germany. Mass spectra of MeCN solutions were recorded with a VG PLATFORM II mass spectrometer. UV−vis spectra were recorded on a Varian Cary 50 UV−vis spectrophotometer. Cyclic voltammograms were recorded using an EG&G Princeton Applied Research 263A potentiostat with a glassy carbon working electrode. Carefully dried and degassed DMF was used as the solvent and $[Bu_4N][PF_6]$ as the supporting electrolyte (0.1 M). All potential values are referenced against the FcH/FcH^+ couple.

Synthesis of ***7***. Neat 3,5-dimethylpyrazole (2.50 g, 26.01 mmol) was slowly added to a stirred suspension of NaH (0.62 g, 25.85 mmol) in THF (100 mL). After 30 min, H_2 evolution had ceased and neat $SOCl_2$ (0.95 mL, 1.55 g, 13.00 mmol) was added in one portion via syringe. After addition of neat 3,4-dihydroxybenzaldehyde (1.80 g, 13.00 mmol) and neat pyridine (10.49 mL, 10.28 g, 130.00 mmol), the reaction mixture was kept at reflux temperature for 12 h. H_2O (50 mL) was added, and the mixture was extracted with CH_2Cl_2 (3 × 50 mL). The combined CH_2Cl_2 extracts were dried over $MgSO_4$ and filtered. The filtrate was evaporated using a rotary evaporator, and the highly viscous oily residue briefly heated to 150 °C on a vacuum line (10^{-3} mbar; heat gun) to remove residual pyridine. EtOAc (100 mL) was added to transform the oil into a colorless solid. Crude **7** was subsequently recrystallized from MeCN/C_6H_6 (5:1) to obtain single crystals. Yield: 1.36 g (33%). ^1H NMR (300.0 MHz, d_6-DMSO): δ 2.08 (s, 6 H; pz-CH_3), 2.10 (d, $^5J_{HH}$ = 0.6 Hz, 6 H; pz-CH_3), 5.87 (s, 2 H; pz-H4), 6.19 (ddd, $^3J_{HH}$ = 8.3 Hz, $^4J_{HH}$ = 2.2 Hz, $^4J_{HH}$ = 0.6 Hz, 1 H; HQ-H6), 6.41 (dd, $^4J_{HH}$ = 2.2 Hz, $^4J_{HH}$ = 0.6 Hz, 1 H; HQ-H2), 6.67 (d, $^3J_{HH}$ = 8.3 Hz, 1 H; HQ-H5), 7.50 (n.r., 1 H; CH), 8.99 (s, 2 H; OH; D_2O-exchangable). ^{13}C NMR (62.9 MHz, d_6-DMSO): δ 11.2, 13.5 (pz-CH_3), 72.6 (Cpz_2), 106.1 (pz-C4), 114.6 (HQ-C2), 115.1 (HQ-C5), 118.0 (HQ-C6), 127.3 (HQ-C1), 140.1 (pz-C5), 145.0, 145.4 (HQ-C3,4), 146.5 (pz-C3). UV−vis (CH_2Cl_2): λ_{max}/nm (ε) 281 (2700). ESI-MS: *m/z* (%) = 215 $[M - Me_2pz - 2H]^-$ (95), 311 $[M - H]^-$ (100). Anal. Calcd for $C_{17}H_{20}N_4O_2$ [312.37]: C 65.37, H 6.45, N 17.94. Found: C 65.54, H 6.24, N 18.09.

Synthesis of ***9***. A mixture of **6** (50 mg, 0.136 mmol) and DDQ (31 mg, 0.136 mmol) was prepared in C_6H_6 (1 mL) at room temperature and stirred for 2 min. The resulting suspension was filtered, and the residue ($DDQH_2$) was washed with C_6H_6 (1 × 1 mL). Freeze-drying of the combined C_6H_6 phases gave **9** as a red-brown powder. Yield: 46 mg (93%). ^1H NMR (300.0 MHz, C_6D_6): δ 1.30 (s, 18 H; CH_3), 5.59 (m, 1 H; BQ-H2), 5.62 (m, 1 H; BQ-H5), 5.87 (ddd, $^3J_{HH}$ = 10.3 Hz, $^4J_{HH}$ = 2.0 Hz, $^4J_{HH}$ = 0.4 Hz, 1 H; BQ-H6), 5.95 (d, $^3J_{HH}$ = 2.5 Hz, 2 H; pz-H4), 6.61 (d, $^4J_{HH}$ = 2.0 Hz, 1 H; CH), 7.02 (d, $^3J_{HH}$ = 2.5 Hz, 2 H; pz-H5). ^{13}C NMR (75.4 MHz, C_6D_6): δ 30.6 (CH_3), 32.5 (CCH_3), 75.9 (Cpz_2), 104.0 (pz-C4), 128.2 (BQ-C2), 129.6 (BQ-C5), 130.0 (pz-C5), 137.0 (BQ-C6), 147.7 (BQ-C1), 164.0 (pz-C3), 178.8, 179.2 (BQ-C3,4). ESI-MS: *m/z* (%) = 368 $[M + H]^+$ (100). Anal. Calcd for $C_{21}H_{26}N_4O_2$ [366.46]·0.25H_2O [18.02]: C 67.99, H 7.20, N 15.10. Found: C 67.58, H 6.82, N 14.76.

Synthesis of ***10***. **7** (200 mg, 0.640 mmol) and $[(MeCN)_2PdCl_2]$ (166 mg, 0.640 mmol) were suspended in MeCN (5 mL), and the suspension was stirred at room temperature for 2.5 h (*note*: this reaction requires neither dry MeCN nor exclusion of air and moisture). After filtration, the filtrate was evaporated to dryness using a rotary evaporator and the residue was briefly heated to 150 °C on a vacuum line (10^{-3} mbar; heat gun) to obtain **10**·H_2O as an orange foam. Yield of **10**·H_2O: 312 mg (96%). Single crystals of **10**·EtOH suitable for X-ray diffraction were grown by slow evaporation of an EtOH solution of **10**·H_2O. ^1H NMR (300.0 MHz, d_3-MeCN): δ 2.46 (d, $^nJ_{HH}$ = 0.4 Hz, 6 H; pz-CH_3), 2.48 (s, 6 H; pz-CH_3), 6.10 (n.r., 2 H; pz-H4), 6.38 (ddd, $^3J_{HH}$ = 8.3 Hz, $^4J_{HH}$ = 2.4 Hz, $^4J_{HH}$ = 0.9 Hz, 1 H; HQ-H6), 6.44 (dd, $^4J_{HH}$ = 2.4 Hz, $^4J_{HH}$ = 0.9 Hz, 1 H; HQ-H2), 6.86 (s, 1 H; OH; D_2O-exchangable), 6.96 (d, $^3J_{HH}$ = 8.3 Hz, 1 H; HQ-H5), 7.15 (s, 1 H; OH; D_2O-exchangable), 7.52 (n.r., 1 H; CH). ^{13}C NMR (75.4 MHz, d_3-MeCN): δ 11.7, 15.2 (pz-CH_3), 70.4 (Cpz_2), 108.9 (pz-C4), 115.1 (HQ-C2), 116.6 (HQ-C5), 120.2 (HQ-C6), 128.3 (HQ-C1), 145.3 (pz-C5), 146.2, 146.6 (HQ-C3,4), 155.0 (pz-C3). UV−vis (CH_2Cl_2): λ_{max}/nm (ε) 281 (3800), 384 (260). Anal. Calcd for $C_{17}H_{20}Cl_2N_4O_2Pd$ [489.69]·H_2O [18.02]: C 40.22, H 4.37, N 11.04. Found: C 39.89, H 4.60, N 10.90.

Synthesis of 11. In a representative procedure, **6** (100 mg, 0.271 mmol) was treated with TlO*t*Bu (151 mg, 0.542 mmol) in THF (2.5 mL) at room temperature. After a clear orange solution had formed, $[(p\text{-cym})RuCl_2]_2$ (83 mg, 0.136 mmol) was added, and the resulting purple suspension was stirred at room temperature overnight. After centrifugation, the supernatant was separated and evaporated to dryness to yield a purple-brown foam. Yield: 163 mg (quant.). Single crystals were grown by gas-phase diffusion of pentane into a THF solution of **11**. ^1H NMR (400.1 MHz, d_8-THF): δ 1.24 (s, 18 H; *t*Bu-CH_3), 1.39 (d, $^3J_{HH}$ = 6.9 Hz, 6 H; *i*Pr-CH_3), 2.29 (s, 3 H; cym-CH_3), 2.76 (sept, $^3J_{HH}$ = 6.9 Hz, 1 H; *i*Pr-CH), 5.80, 5.84 (2 × d, 2 × $^3J_{HH}$ = 6.0 Hz, 2 × 2 H; cym-H), 6.04 (d, $^3J_{HH}$ = 2.4 Hz, 2 H; pz-H4), 6.25 (dd, $^3J_{HH}$ = 8.3 Hz, $^4J_{HH}$ = 1.9 Hz, 1 H; HQ-H6), 6.55 (d, $^4J_{HH}$ = 1.9 Hz, 1 H; HQ-H2), 6.80 (d, $^3J_{HH}$ = 8.3 Hz, 1 H; HQ-H5), 7.26 (d, $^3J_{HH}$ = 2.4 Hz, 2 H; pz-H5), 7.41 (s, 1 H; CH). ^{13}C NMR (100.6 MHz, d_8-THF): δ 19.4 (cym-CH_3), 23.3 (*i*Pr-CH_3), 31.0 (*t*Bu-CH_3), 32.8 (*i*Pr-CH), 33.1 (*t*Bu-CCH_3), 75.1, 77.2 (cym-C2,3,5,6), 79.2 (Cpz_2), 90.6, 99.8 (cym-C1,4), 102.2 (pz-C4), 115.4 (HQ-C2), 116.0 (HQ-C5), 117.7 (HQ-C6), 128.3 (HQ-C1), 130.1 (pz-C5), 162.2 (pz-C3), 164.3, 165.0 (HQ-C3,4). UV−vis (CH_2Cl_2): λ_{max}/nm (ε): 287 (45 100), 323 (27 700), 490 (46 300). ESI-MS: *m/z* (%) = 602 $[M + H]^+$ (100). Anal. Calcd for $C_{31}H_{40}N_4O_2Ru$ [601.74]: C 61.88, H 6.70, N 9.31. Found: C 61.87, H 6.74, N 9.18.

Synthesis of ***12***. Following the general procedure outlined for the synthesis of **11**, **7** (30 mg, 0.096 mmol) was treated with TlO*t*Bu (53 mg, 0.191 mmol) and $[(ppy)_2IrCl]_2$ (52 mg, 0.048 mmol) in THF

dx.doi.org/10.1021/om3000746 | *Organometallics* 2012, 31, 3213−3221

(2.0 mL) to obtain a red solid. Yield: 98 mg (quant.). Single crystals suitable for X-ray diffraction were grown from a saturated EtCN solution of **12**. Some ^{1}H NMR signals are poorly resolved, due to the presence of two isomers with very similar chemical shift values. An unambiguous assignment of the signals to the individual isomers is not possible. ^{1}H NMR (300.0 MHz, d_8-THF): δ 1.96, 2.06 (2 × bs, 2 × 6 H; 2 × pz-CH_3), 2.18, 2.22 (2 × s, 2 × 6 H; 2 × pz-CH_3), 5.03 (n.r., 2 H; HQ-H), 5.71, 5.80 (2 × s, 2 × 2 H; 2 × pz-H4), 5.94 (n.r., 2 H; HQ-H), 6.08, 6.28 (2 × m, 2 × 2 H; 2 × ppy-H), 6.45, 6.67 (2 × m, 2 × 4 H; ppy-H), 6.91, 6.99 (2 × n.r., 2 × 2 H; 2 × ppy-H), 7.25 (bs, 2 H; CH), 7.44, 7.54, 7.75 (3 × m, 3 × 4 H; ppy-H), 8.79, 8.90 (2 × n.r., 2 × 2 H; 2 × ppy-H), n.o. HQ-H. The two different isomers lead to two sets of ^{13}C NMR signals with very similar chemical shift values; in some cases, not all signals are resolved, so that the number of resonances listed does not equal twice the number of C atoms. ^{13}C NMR (100.6 MHz, d_8-THF): δ 11.3, 11.5 (pz-CH_3), 13.8, 14.0 (pz-CH_3), 71.8 (Cpz_2), 105.8, 106.3 (pz-C4), 113.3 (HQ-C), 115.2 (HQ-C), 118.6, 120.3, 120.6, 121.8, 124.3, 124.6 (4 × ppy-C), 127.5 (HQ-C1), 129.2, 134.1, 135.3, 136.6, 136.8 (3 × ppy-C), 140.9, 141.5 (pz-C3,5), 148.2, 149.1, 149.9, 153.0 (4 × ppy-C), 169.1, 169.6 (HQ-C3,4), n.o. HQ-C, ppy-C1. UV−vis (CH_2Cl_2): λ_{max}/nm (ε): 370 (14 900), 451 (8200), 524 (4200). ESI-MS: m/z (%) = 811 $[M - Tl]^-$ (100). Anal. Calcd for $C_{39}H_{34}IrN_6O_2Tl$ [1015.33]: C 46.13, H 3.38, N 8.28. Found: C 46.14, H 3.21, N 8.49.

Synthesis of ***14****.* Following the representative procedure outlined for the synthesis of **11**, **7** (100 mg, 0.320 mmol) was treated with Tl*O*t*Bu* (178 mg, 0.640 mmol) and $[(Cp^*)IrCl_2]_2$ (128 mg, 0.160 mmol) in THF (2.0 mL) to obtain a brick-red solid. Yield: 179 mg (88%). Structure determination was performed on a single crystal grown by slow evaporation of a THF solution of **14**. ^{1}H NMR (300.0 MHz, d_8-THF): δ 1.88 (s, 15 H; Cp*-CH_3), 2.10 (s, 6 H; pz-CH_3), 2.13 (d, $^n J_{HH}$ = 0.7 Hz, 6 H; pz-CH_3), 5.73 (n.r., 2 H; pz-H4), 6.17 (ddd, $^3J_{HH}$ = 8.3 Hz, $^4J_{HH}$ = 2.0 Hz, $^4J_{HH}$ = 0.7 Hz, 1 H; HQ-H6), 6.36 (dd, $^4J_{HH}$ = 2.0 Hz, $^4J_{HH}$ = 0.7 Hz, 1 H; HQ-H2), 6.77 (d, $^3J_{HH}$ = 8.3 Hz, 1 H; HQ-H5), 7.58 (n.r., 1 H; CH). ^{13}C NMR (75.4 MHz, d_8-THF): δ 10.2 (Cp*-CH_3), 12.1, 13.8 (pz-CH_3), 75.2 (Cpz_2), 85.2 (Cp*), 106.4 (pz-C4), 113.6 (HQ-C2), 114.1 (HQ-C5), 117.0 (HQ-C6), 127.2 (HQ-C1), 141.2 (pz-C5), 147.5 (pz-C3), 165.0, 165.2 (HQ-C3,4). UV−vis (CH_2Cl_2): λ_{max}/nm (ε) 287 (13 100), 429 (22 800). ESI-MS: m/z (%) = 678 $[M + MeCN + H]^+$ (100). Anal. Calcd for $C_{27}H_{33}IrN_4O_2$ [637.79]: C 50.85, H 5.22, N 8.78. Found: C 50.79, H 5.33, N 8.58.

Synthesis of ***16****.* **14** (13 mg, 0.020 mmol) and $[(MeCN)_2PdCl_2]$ (5 mg, 0.020 mmol) were placed into a flame-dried NMR tube, and d_3-MeCN (0.75 mL) was added. The tube was flame-sealed under vacuum and heated to 150 °C for 2 min with shaking (heat gun). After that time, ^{1}H NMR spectroscopy indicated full consumption of the starting materials with formation of **16** in ca. 90% purity. The NMR tube was centrifuged and opened, and the solution was evaporated to dryness under vacuum. The residue was placed into a new NMR tube and dissolved in THF (1 mL), and the solution was stored at room temperature overnight without exclusion of air and moisture to obtain red X-ray quality crystals. Yield of single crystals: 13 mg (73%). To prepare a sample for the combustion analysis, some crystals were washed with Et_2O and then stored at room temperature under vacuum for several hours. ^{1}H NMR (300.0 MHz, d_3-MeCN): δ 1.90 (s, 15 H; Cp*-CH_3), 2.43, 2.49 (2 × s, 2 × 6 H; pz-CH_3), 6.08 (n.r., 2 H; pz-H4), 6.20 (ddd, $^3J_{HH}$ = 8.3 Hz, $^4J_{HH}$ = 2.3 Hz, $^4J_{HH}$ = 1.0 Hz, 1 H; HQ-H6), 6.41 (dd, $^4J_{HH}$ = 2.3 Hz, $^4J_{HH}$ = 1.0 Hz, 1 H; HQ-H2), 7.00 (d, $^3J_{HH}$ = 8.3 Hz, 1 H; HQ-H5), 7.53 (n.r., 1 H; CH). ^{13}C NMR (100.6 MHz, d_3-MeCN): δ 10.6 (Cp*-CH_3), 11.7, 15.3 (pz-CH_3), 70.8 (Cpz_2), 86.4 (Cp*), 108.8 (pz-C4), 113.0 (HQ-C2), 115.0 (HQ-C5), 117.8 (HQ-C6), 125.7 (HQ-C1), 145.1, 154.9 (pz-C3,5), 164.9, 165.8 (HQ-C3,4). UV−vis (CH_2Cl_2): λ_{max}/nm (ε): 289 (7100), 422 (13 500). ESI-MS: m/z (%) = 850 $[M + Cl]^-$ (6). Anal. Calcd for $C_{27}H_{33}Cl_2IrN_4O_2Pd$ [815.12]·0.5C_4H_8O [72.11]: C 40.92, H 4.38, N 6.58. Found: C 40.93, H 4.14, N 7.01.

X-ray Crystallography of 7, 8, 10, 11, 12, 14, 15, and 16. Data collections were performed on Stoe IPDS-II two-circle diffractometers either with graphite-monochromated Mo Kα (**7**, **10**, **11**, **12**, **14**, **15**, **16**) or with graphite-monochromated Cu Kα radiation (**8**). In all cases, repeatedly measured reflections remained stable. Empirical absorption corrections were performed for **10**, **11**, **12**, **14**, **15**, and **16** using the MULABS[37] option in PLATON.[38] Equivalent reflections were averaged. The structures were solved by direct methods using the program SHELXS[39] and refined with full-matrix least-squares on F^2 using the program SHELXL-97.[40] If not mentioned otherwise, hydrogen atoms were placed on ideal positions and refined with fixed isotropic displacement parameters using a riding model.

In **7**, the H atoms bonded to O were freely refined. For **10**, the absolute structure was determined by refining the Flack parameter to a value of −0.02(2); the C−C−O−H torsion angles were refined. In **12**, the displacement ellipsoids of the atoms N12A and C16A and of the three EtCN molecules were restrained to an isotropic behavior. In **14**, one of the THF molecules was refined with the O−C distances restrained to 1.40(1) Å and the C−C distances restrained to 1.50(1) Å; angle distances in both THF molecules were restrained to 2.3(1) Å. In **15**, one of the *t*Bu groups is disordered over two positions with a site occupation factor of 0.57(1) for the major occupied site. In **16**, one C atom of the THF molecule is disordered over two positions with a site occupation factor of 0.58(6) for the major occupied site; the H atom of cocrystallized water was isotropically refined with the O−H distance restrained to 0.82(1) Å.

CCDC reference numbers: 864576 (**7**), 864577 (**8**), 864578 (**10**), 864579 (**11**), 864580 (**12**), 864581 (**14**), 864582 (**15**), 864583 (**16**).

■ ASSOCIATED CONTENT

Ⓢ Supporting Information

NMR spectroscopic data of **6** in C_6D_6, synthesis and analytical data of **8**, **13**, and **15**; X-ray crystal structure analysis of **8**, **11**, and **15**; cyclic voltammetry on **6**, **14**, and **16**. This material is available free of charge via the Internet at http://pubs.acs.org.

■ AUTHOR INFORMATION

Corresponding Author

*E-mail: Matthias.Wagner@chemie.uni-frankfurt.de.

Notes

The authors declare no competing financial interest.

■ ACKNOWLEDGMENTS

This research was supported by the Deutsche Forschungsgemeinschaft (SFB/TR 49). F.B. is grateful to the Fonds der Chemischen Industrie (FCI) for a Ph.D. grant. The authors wish to thank Prof. Dr. A. Schmidt (Technische Universität Clausthal, Germany) for helpful discussions on *ortho*-benzoquinone trapping reactions and Dr. Dieter Schollmeyer (Johannes Gutenberg-Universität Mainz, Germany) for acquiring the X-ray data set of compound **8**.

■ REFERENCES

(1) Wilcox, D. E. *Chem. Rev.* **1996**, *96*, 2435−2458.
(2) Sträter, N.; Lipscomb, W. N.; Klabunde, T.; Krebs, B. *Angew. Chem., Int. Ed. Engl.* **1996**, *35*, 2024−2055.
(3) Steinhagen, H.; Helmchen, G. *Angew. Chem., Int. Ed. Engl.* **1996**, *35*, 2339−2342.
(4) Vance, D. H.; Czarnik, A. W. *J. Am. Chem. Soc.* **1993**, *115*, 12165−12166.
(5) Liu, S.; Luo, Z.; Hamilton, A. D. *Angew. Chem., Int. Ed. Engl.* **1997**, *36*, 2678−2680.
(6) Ritter, J. C. M.; Bergman, R. G. *J. Am. Chem. Soc.* **1998**, *120*, 6826−6827.
(7) Angamuthu, R.; Byers, P.; Lutz, M.; Spek, A. L.; Bouwman, E. *Science* **2010**, *327*, 313−315.
(8) Smith, A. L.; Hardcastle, K. I.; Soper, J. D. *J. Am. Chem. Soc.* **2010**, *132*, 14358−14360.

(9) Konsler, R. G.; Karl, J.; Jacobsen, E. N. *J. Am. Chem. Soc.* **1998**, *120*, 10780−10781.
(10) (a) Dinnebier, R.; Lerner, H.-W.; Ding, L.; Shankland, K.; David, W. I. F.; Stephens, P. W.; Wagner, M. *Z. Anorg. Allg. Chem.* **2002**, *628*, 310−314. (b) Ma, K.; Scheibitz, M.; Scholz, S.; Wagner, M. *J. Organomet. Chem.* **2002**, *652*, 11−19. (c) Bieller, S.; Haghiri, A.; Bolte, M.; Bats, J. W.; Wagner, M.; Lerner, H.-W. *Inorg. Chim. Acta* **2006**, *359*, 1559−1572. (d) Margraf, G.; Kretz, T.; Fabrizi de Biani, F.; Laschi, F.; Losi, S.; Zanello, P.; Bats, J. W.; Wolf, B.; Remović-Langer, K.; Lang, M.; Prokofiev, A.; Assmus, W.; Lerner, H.-W.; Wagner, M. *Inorg. Chem.* **2006**, *45*, 1277−1288. (e) Lerner, H.-W.; Margraf, G.; Kretz, T.; Schiemann, O.; Bats, J. W.; Dürner, G.; Fabrizi de Biani, F.; Zanello, P.; Bolte, M.; Wagner, M. *Z. Naturforsch.* **2006**, *61b*, 252−264. (f) Kretz, T.; Bats, J. W.; Losi, S.; Wolf, B.; Lerner, H.-W.; Lang, M.; Zanello, P.; Wagner, M. *Dalton Trans.* **2006**, 4914−4921. (g) Ruth, K.; Tüllmann, S.; Vitze, H.; Bolte, M.; Lerner, H.-W.; Holthausen, M. C.; Wagner, M. *Chem.—Eur. J.* **2008**, *14*, 6754−6770. (h) Phan, N. H.; Halasz, I.; Opahle, I.; Alig, E.; Fink, L.; Bats, J. W.; Cong, P. T.; Lerner, H.-W.; Sarkar, B.; Wolf, B.; Jeschke, H. O.; Lang, M.; Valentí, R.; Dinnebier, R.; Wagner, M. *Cryst. Eng. Comm.* **2011**, *13*, 391−395.
(11) For an overview of scorpionate ligands see: (a) Trofimenko, S. *Scorpionates−The Coordination Chemistry of Polypyrazolylborate Ligands*; Imperial College Press: London, 1999. (b) Pettinari, C. *Scorpionates II: Chelating Borate Ligands*, 1st ed.; Imperial College Press: London, 2008.
(12) (a) Jäkle, F.; Polborn, K.; Wagner, M. *Chem. Ber.* **1996**, *129*, 603−606. (b) Fabrizi de Biani, F.; Jäkle, F.; Spiegler, M.; Wagner, M.; Zanello, P. *Inorg. Chem.* **1997**, *36*, 2103−2111. (c) Herdtweck, E.; Peters, F.; Scherer, W.; Wagner, M. *Polyhedron* **1998**, *17*, 1149−1157. (d) Guo, S. L.; Peters, F.; Fabrizi de Biani, F.; Bats, J. W.; Herdtweck, E.; Zanello, P.; Wagner, M. *Inorg. Chem.* **2001**, *40*, 4928−4936. (e) Guo, S. L.; Bats, J. W.; Bolte, M.; Wagner, M. *J. Chem. Soc., Dalton Trans.* **2001**, 3572−3576. (f) Haghiri Ilkhechi, A.; Guo, S.; Bolte, M.; Wagner, M. *Dalton Trans.* **2003**, 2303−2307. (g) Bieller, S.; Zhang, F.; Bolte, M.; Bats, J. W.; Lerner, H.-W.; Wagner, M. *Organomet.* **2004**, *23*, 2107−2113. (h) Zhang, F.; Bolte, M.; Lerner, H.-W.; Wagner, M. *Organometallics* **2004**, *23*, 5075−5080. (i) Haghiri Ilkhechi, A.; Scheibitz, M.; Bolte, M.; Lerner, H.-W.; Wagner, M. *Polyhedron* **2004**, *23*, 2597−2604. (j) Haghiri Ilkhechi, A.; Bolte, M.; Lerner, H.-W.; Wagner, M. *J. Organomet. Chem.* **2005**, *690*, 1971−1977. (k) Haghiri Ilkhechi, A.; Mercero, J. M.; Silanes, I.; Bolte, M.; Scheibitz, M.; Lerner, H.-W.; Ugalde, J. M.; Wagner, M. *J. Am. Chem. Soc.* **2005**, *127*, 10656−10666. (l) Bieller, S.; Bolte, M.; Lerner, H.-W.; Wagner, M. *Inorg. Chem.* **2005**, *44*, 9489−9496. (m) Bieller, S.; Bolte, M.; Lerner, H.-W.; Wagner, M. *Chem.—Eur. J.* **2006**, *12*, 4735−4742. (n) Kunz, K.; Vitze, H.; Bolte, M.; Lerner, H.-W.; Wagner, M. *Organomet.* **2007**, *26*, 4663−4672. (o) Zhang, F.; Morawitz, T.; Bieller, S.; Bolte, M.; Lerner, H.-W.; Wagner, M. *Dalton Trans.* **2007**, 4594−4598. (p) Morawitz, T.; Bolte, M.; Lerner, H.-W.; Wagner, M. *Z. Anorg. Allg. Chem.* **2008**, *634*, 1409−1414. (q) Morawitz, T.; Bolte, M.; Lerner, H.-W.; Wagner, M. *Z. Anorg. Allg. Chem.* **2008**, *634*, 1570−1574. (r) Morawitz, T.; Zhang, F.; Bolte, M.; Bats, J. W.; Lerner, H.-W.; Wagner, M. *Organomet.* **2008**, *27*, 5067−5074. (s) Morawitz, T.; Bao, S.; Bolte, M.; Lerner, H.-W.; Wagner, M. *J. Organomet. Chem.* **2008**, *693*, 3878−3884. (t) Kaufmann, L.; Haghiri Ilkhechi, A.; Vitze, H.; Bolte, M.; Lerner, H.-W.; Wagner, M. *J. Organomet. Chem.* **2009**, *694*, 466−472. (u) Mutseneck, E. V.; Reus, C.; Schödel, F.; Bolte, M.; Lerner, H.-W.; Wagner, M. *Organometallics* **2010**, *29*, 966−975. (v) Kunz, K.; Bolte, M.; Lerner, H.-W.; Wagner, M. *Organometallics* **2009**, *28*, 3079−3087. (w) Mutseneck, E. V.; Bieller, S.; Bolte, M.; Lerner, H.-W.; Wagner, M. *Inorg. Chem.* **2010**, *49*, 3540−3552. (x) Reus, C.; Ruth, K.; Tüllmann, S.; Bolte, M.; Lerner, H.-W.; Weber, B.; Holthausen, M. C.; Wagner, M. *Eur. J. Inorg. Chem.* **2011**, 1709−1718.
(13) For a review on bis(pyrazol-1-yl)methane ligands see: Pettinari, C.; Pettinari, R. *Coord. Chem. Rev.* **2005**, *249*, 663−691.
(14) Scheuermann, S.; Kretz, T.; Vitze, H.; Bats, J. W.; Bolte, M.; Lerner, H.-W.; Wagner, M. *Chem.—Eur. J.* **2008**, *14*, 2590−2601.
(15) Scheuermann, S.; Sarkar, B.; Bolte, M.; Bats, J. W.; Lerner, H.-W.; Wagner, M. *Inorg. Chem.* **2009**, *48*, 9385−9392.
(16) Blasberg, F.; Bats, J. W.; Bolte, M.; Lerner, H.-W.; Wagner, M. *Inorg. Chem.* **2010**, *49*, 7435−7445.
(17) Blasberg, F.; Bolte, M.; Wagner, M.; Lerner, H.-W. *J. Organomet. Chem.* **2011**, *696*, 3593−3600.
(18) Wunderlich, H.; Mootz, D. *Acta Crystallogr.* **1971**, *B27*, 1684−1686.
(19) Macdonald, A. L.; Trotter, J. *J. Chem. Soc., Perkin Trans. 2* **1973**, 476−480.
(20) Willstätter, R.; Pfannenstiel, A. *Ber. Dtsch. Chem. Ges.* **1904**, *37*, 4744−4746.
(21) Schmidt, A.; Mordhorst, T.; Nieger, M. *Nat. Prod. Res.* **2005**, *19*, 541−546.
(22) Schmidt, A.; Topp, M.; Mordhorst, T.; Schneider, O. *Tetrahedron* **2007**, *63*, 1842−1848.
(23) Schmidt, A.; Albrecht, M.; Mordhorst, T.; Topp, M.; Jeschke, G. *J. Mater. Chem.* **2007**, *17*, 2793−2800.
(24) Oxidative addition of low-valent metal complex fragments to **9** to yield catecholate complexes is subject to further studies.
(25) Sánchez-Méndez, A.; de Jesús, E.; Flores, J. C.; Gómez-Sal, P. *Eur. J. Inorg. Chem.* **2010**, 141−151.
(26) Steinborn, D. *Fundamentals of Organometallic Catalysis*, 1st ed.; Wiley-VCH: Weinheim, 2011.
(27) (a) Habereder, T.; Warchhold, M.; Nöth, H.; Severin, K. *Angew. Chem., Int. Ed.* **1999**, *38*, 3225−3228. (b) Piotrowski, H.; Polborn, K.; Hilt, G.; Severin, K. *J. Am. Chem. Soc.* **2001**, *123*, 2699−2700. (c) Lehaire, M.-L.; Scopelliti, R.; Piotrowski, H.; Severin, K. *Angew. Chem., Int. Ed.* **2002**, *41*, 1419−1422. (d) Lehaire, M.-L.; Scopelliti, R.; Severin, K. *Inorg. Chem.* **2002**, *41*, 5466−5474. (e) Lehaire, M.-L.; Scopelliti, R.; Herdeis, L.; Polborn, K.; Mayer, P.; Severin, K. *Inorg. Chem.* **2004**, *43*, 1609−1617. (f) Grote, Z.; Scopelliti, R.; Severin, K. *J. Am. Chem. Soc.* **2004**, *126*, 16959−16972. (g) Shanmugaraju, S.; Bar, A. K.; Joshi, S. A.; Patil, Y. P.; Mukherjee, P. S. *Organometallics* **2011**, *30*, 1951−1960. (h) Ozawa, H.; Hino, T.; Ohtsu, H.; Wada, T.; Tanaka, K. *Inorg. Chim. Acta* **2011**, *366*, 298−302.
(28) Blasberg, F.; Lerner, H.-W.; Bolte, M. *Acta Crystallogr.* **2010**, *E66*, m1621.
(29) Lowry, M. S.; Hudson, W. R.; Pascal, R. A. Jr.; Bernhard, S. *J. Am. Chem. Soc.* **2004**, *126*, 14129−14135.
(30) Flamigni, L.; Barbieri, A.; Sabatini, C.; Ventura, B.; Barigelletti, F. *Top. Curr. Chem.* **2007**, *281*, 143−203.
(31) Panichakul, D.; Su, Y.; Li, Y.; Deng, W.; Zhao, J.; Li, X. *Organometallics* **2008**, *27*, 6390−6392.
(32) Childress, M. V.; Millar, D.; Alam, T. M.; Kreisel, K. A.; Yap, G. P. A.; Zakharov, L. N.; Golen, J. A.; Rheingold, A. L.; Doerrer, L. H. *Inorg. Chem.* **2006**, *45*, 3864−3877.
(33) Mathur, R. S.; Drovetskaya, T.; Reed, C. A. *Acta Crystallogr.* **1997**, *C53*, 881−883.
(34) Kunz, K.; Blasberg, F.; Bolte, M.; Lerner, H.-W.; Wagner, M. *Inorg. Chim. Acta* **2009**, *362*, 4372−4376.
(35) Nomura, M.; Kusui, A.; Kajitani, M. *Organometallics* **2005**, *24*, 2811−2818.
(36) Blasberg, F.; Bats, J. W.; Wagner, M.; Lerner, H.-W. *Acta Crystallogr.* **2011**, *E67*, m1837−m1838.
(37) Blessing, R. H. *Acta Crystallogr.* **1995**, *A51*, 33−38.
(38) Spek, A. L. *J. Appl. Crystallogr.* **2003**, *36*, 7−13.
(39) Sheldrick, G. M. *Acta Crystallogr.* **1990**, *A46*, 467−473.
(40) Sheldrick, G. M. *SHELXL-97, Program for the Refinement of Crystal Structures*; Universität Göttingen: Göttingen, Germany, 1997.